Application of Surface Enhanced Raman Spectroscopy to the Study of SOFC Electrode Surfaces

Xiaxi Li, Kevin Blinn, Yingcui Fang, Mingfei Liu, Mahmoud A. Mahmoud, Shuang Cheng, Lawrence A. Bottomley, Mostafa El-Sayed, and Meilin Liu

Electronic Supplementary Information

This document provides further detail on the following aspects of our study:

A. Sample preparation

B. Evaluation of the SERS effect

C. Optimization of enhancement factor

D. Discussions

A. Preparation of Samples

Carbon Film Standards: To systematically explore the silver sputtering condition that gives optimum enhancement for the underlying substrate, carbon films of uniform thickness were deposited onto glass cover slips as the standards. Carbon evaporation was conducted in a vacuum evaporator (Quarum Technique), with a typical working pressure of 7×10^{-5} mBar. Carbon rods with a sharpened tip (Ted Pella) were used as the evaporation source. The evaporator's stage has a rotation mechanism which ensured the uniformity of carbon deposition. The thicknesses of the standard carbon films fabricated in the same batch were generally uniform, which was confirmed by Raman spectroscopy and AFM.

Coked Nickel Surface: Nickel plates exposed to hydrocarbon-containing atmosphere were used to simulate the nickel anode used in SOFCs. Nickel foils (Alfa Aesar) were first cut into small square coupons with sizes of ~8 mm, and then polished to reach a grade of 0.1 μm. The polished samples were subsequently sonicated in acetone, ethanol, and water to remove any residues on the polished surface. The nickel surface was exposed to mixed gas composed of 15% H_2 and 10% propane in argon in a quartz tube at 550ºC for 2 minutes to build up carbon deposition.

Other SOFC related Materials: To fabricate a CeO_2-modified nickel surface, we performed electrochemical deposition on a clean nickel foil. $La_1Sr_{0.4}Co_{0.2}Fe_{0.8}O_{3-\delta}$ (LSCF) pellets were fabricated by dry pressing of LSCF powder (Fuel Cell Materials) and firing at 1350 ºC for 7 hrs. A $La_xSr_yMnO_{3-\delta}$ (LSM) thin film was deposited on a polished yttrium-stabilized zirconia (YSZ) substrate through RF sputtering followed by thermal annealing at 800 ºC for 1 hr.

Creating SERS active silver agent by DC Sputtering: Silver was deposited onto the substrates through DC magnetron sputtering. Prior to deposition, the chamber was pumped to a pressure level lower than 6.3×10^{-6} mBar, followed by introduction of argon to reach the designated working pressures. To preserve the original state of the surface species as much as possible, we did not heat up the sample stage, and the heating due to electron bombardment was likely negligible due to the low power and short duration. Sputtering power, working pressure, and deposition time were varied to explore the optimal sputtering condition. For each parameter point of silver sputtering, a carbon coated silicon wafer (for Raman and SEM characterization) and a blank glass coverslip (for UV-Vis absorption spectrum) were used as substrates.

B. Evaluation of the SERS effect (Raman, SEM and UV-Vis)

Raman spectra were obtained using a Renishaw RM 1000 spectromicroscopy system (~2 µm spot size). 514 nm and 633 nm laser wavelengths were used for excitation in this study. The Raman signal was collected by a CCD array, and the average integration times were 100 s for 514 nm excitation and 500 s for 633 nm.

SERS enhancement factors (EF) were evaluated in different ways when the species of interest are underneath the silver particles (the cases of carbon film, coked nickel and other SOFC materials) and when it is loaded on top of the silver particles (R6G dye). The EF calculated on carbon films is taken as the ratio of the carbon peak intensity after silver loading to the original intensity:

$$EF_{net} = \frac{I_{SERS}}{I_{Blank}}$$

We did not further normalize this net EF by factors such as exposed surface area of the substrate and the carbon species far from the particles that are inactive for SERS, which could generate a much larger value, since our goal was to optimize the signal output for our further application.

To compare our work with the previous SERS studies, we employed R6G as another reporter of SERS effect. To effectively control the surface concentration of the R6G loaded onto the substrate for the evaluation of enhancement factor, equal amount (15µL) of R6G solution of certain concentration was dropped into a space on the substrates with equal area (0.19cm^2). The area of the space was defined by a BUNA rubber O-Ring, which was secured onto the substrate with two binder clips and a metal washer between the clips and O-ring to distribute the force evenly. The Raman spectra were collected after the solution was evaporated. We calculated the EF of R6G with a similar method proposed by Le Ru [1] and Van Duyne[2]:

$$EF_0 = \frac{I_{SERS}}{I_{Bulk}} \times \frac{N_{Bulk}}{N_{SERS}}$$

N is the number of R6G molecules being probed by the laser beam, and I is the intensity of the R6G main peak (1390cm^{-1}). On both the SERS substrate and blank substrate (Bulk), the deposited R6G molecule films are thin enough (nominal thickness is less than 20nm for 7x10^{-9}Mol/cm^2), so we can assume all the molecules in the laser spot contribute to the Raman signal equally and the correction of N_{vol} with respect to the penetration depth may not be needed [1, 3]. The value of N in both cases can be estimated by:

$$N_i = \sigma_i A = \frac{15\mu L}{0.19cm^2} c_i A$$

σ_i is the surface concentration of the R6G molecules; A is the area of the laser spot; c_i is the concentration of the solution loaded onto the substrate, which is 10^{-7}M for SERS substrate and 10^{-4}M for the blank Si wafer. According to the spectra shown in the Figure 2 of main text, the EF$_0$ was calculated to be 4x10^5.

Since we did not consider the factor of silver surface roughness and whether nanometer scale homogeneity of R6G absorption on silver, this figure may not be the intrinsic enhancement factor of our SERS substrate, but it serves as a good indicator to be compared with previous SERS studies.

To image the surface morphology of the sputtered silver film, a LEO 1530 Scanning electron microscope was used. Only high magnification images are shown in this document, but we ensured the uniformity of the silver loading across the sample surface by examination of low magnification images.

Absorption spectra of the silver nanoparticles were collected on a UV-Vis-NIR spectrometer (Ocean Optics) with its wavelength ranging from 200 to 1200 nm. The absorption at each wavelength was calculated by the following algorithm[4]:

$$A = -\log \frac{E_{st} - E_{dark}}{E_{air} - E_{dark}}$$

E_{dark} is the voltage in the photo diode when the laser is fully blocked, E_{air} is collected when there is only air between the laser source and photo diode, and E_{st} is collected when sample is placed in between the source and diode. For each spectrum, 100 collections with each lasting for 23 ms are averaged.

C. Optimization of the enhancement factor

According to the relevant literature[5-9], the primary factors that influence the film morphology and the corresponding optical properties are working pressure, power, duration, and the heat treatment of the substrates. To use SERS as a tool for surface inspection, the substrate needs to be kept at room temperature or the surface species will dissociate or transform. Additionally, we found that changing power did not have significant impact on the film morphology, if the change of deposition rate is compensated by the change of deposition duration. Therefore, in the subsequent parameter exploration, we kept a constant power output of 8W.

To explore the impact of deposition duration and working pressure, a 3 by 3 full factorial experiment was first conducted. The deposition duration was tested in 3 levels (60, 120 and 180 s) and the working pressure was also varied in 3 levels (1, 2.5, and 5 x 10^{-2} mBar). The sample from each of these parameter points was characterized by SEM, UV-Vis absorption spectroscopy and Raman spectroscopy. Based on the results of this set of parameters, a few more points were explored to search for the optimal condition, which were: 120 s at 0.5 x 10^{-2} mBar, 240 s at 2.5 x 10^{-2} mBar and 300s at 2.5 x 10^{-2} mBar. The SEM images (Figure S-1), UV-Vis absorption spectra (Figure S-2) and SERS spectra (Figure S-3) are all arranged according to their deposition times and working pressures.

D. Discussions

The SEM images presented in Figure S-1 show that silver loading increased with longer sputtering duration and with lower working pressure. The negative correlation between the working pressure and deposition amount can be explained by the decreased mean free path at high working pressure [10]. It is worth noticing that when the loading amount was too high, particularly in the case of 180 s at 1 Pa, the nanoparticles agglomerated into a network. As will be shown below, such agglomeration of nanoparticles changed the resonance spectrum of the silver, and thus diminished the Raman enhancement.

Figure S-2 shows the UV-Vis absorption spectra of the silver particles loaded on carbon buffered glass and blank glass which were used to characterize the interaction between incident light and silver particles. According to the Mie approximation of Maxwell equation, local surface plasmon resonance (LSPR) can be excited when the wavelength of the incident light meet certain requirement with respect to the properties of the silver nanoparticles[11]. The resonance generates stronger electromagnetic field at the vicinity of the particles, which is responsible for enhancement of the Raman signal. For a maximum SERS effect, the LSPR peak of the substrate should be in between the wavelength of incident laser and that of Raman scattered light[12]. These “active regions” determined by the incident laser and the species in which we are interested are indicated by two shaded boxes on the UV-Vis background. For 633 nm incident light, the optimal LSPR wavelength for SERS should be between 633 nm and 703 nm (G-band Raman shift for 633 nm); for 514 nm excitation, the maximum SERS occurs when LSPR wavelength lies between 514 nm and 560 nm.

The LSPR wavelength can be fine tuned by the geometry of nanoparticles[13]: when the size of metal particle increases, the absorption peak shifts to longer wavelength. By comparing Figure S-1 and Figure S-2, we found longer LSPR wavelength when the particle size increases, which is consistent with the Mie solution. We also observed higher absorption ratio at higher loading, which can be attributed to the increased loading of silver. In the cases when the size of silver particles becomes large enough and interconnecting network is formed, the adsorption spectra no longer display resonance peaks.

The Raman spectra of each of the aforementioned parameters are shown in Figure S-3. In each frame, the black dashed line represents the baseline of normal Raman spectrum, which is not very sensitive to the excitation laser wavelength. The red and green bolded lines are the Raman signal after SERS treatment, collected by red (633nm) and green (514nm) lasers, respectively. The baseline was normalized to a peak intensity of 1000 counts, and the adjustment factor was applied to the SERS spectra.

The enhancement factor given by green laser was much higher than that provided by red laser, which was consistent with the UV-Vis absorption spectra: the LSPR wavelength was close to 514 nm rather than 633 nm, so a much higher plasmon field can be achieved when excited at 514 nm. Comparing Figure S-2 and Figure S-3, it is apparent that the enhancement factor scales with the absorption intensity at the vicinity of incident light. However, in the cases when interconnecting network formed and no UV-Vis absorption peak was displayed, the Raman enhancement dropped significantly. The correlation between absorption coefficient and the SERS EF is further shown in Figure S-4, by plotting all the samples that did not form the interconnecting particles. Linear trends can be observed on both plots.

In summary, the optical properties of the silver nanoparticles can be tuned by adjusting the sputter duration and working pressure. Shorter duration and high working pressure gives smaller silver particles with the SPR peak at shorter wavelength, and provides smaller enhancement. On the contrary, longer duration and low working pressure gives larger silver particles with long wavelength SPR peaks and generate stronger SERS effect. However, too high silver loading makes the particles agglomerated into a network, which changes the light absorption behavior of the sample and covers too much of the species underneath, diminishing a portion of the SERS effect.

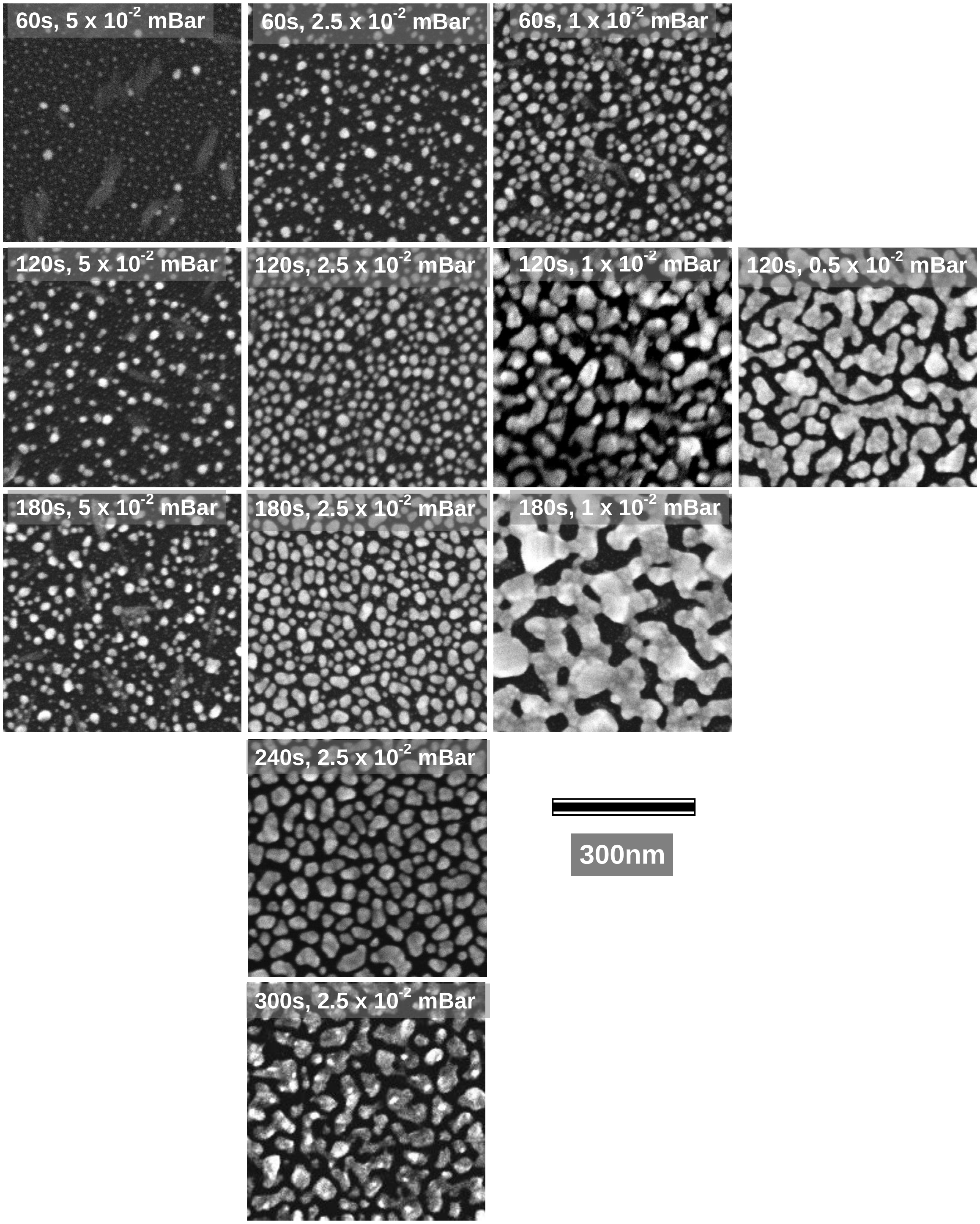

Figure S-1. SEM images of silver sputtered on carbon coated silicon substrates. The annotations indicate the duration and the working pressure of silver sputtering. All images are of the same scale.

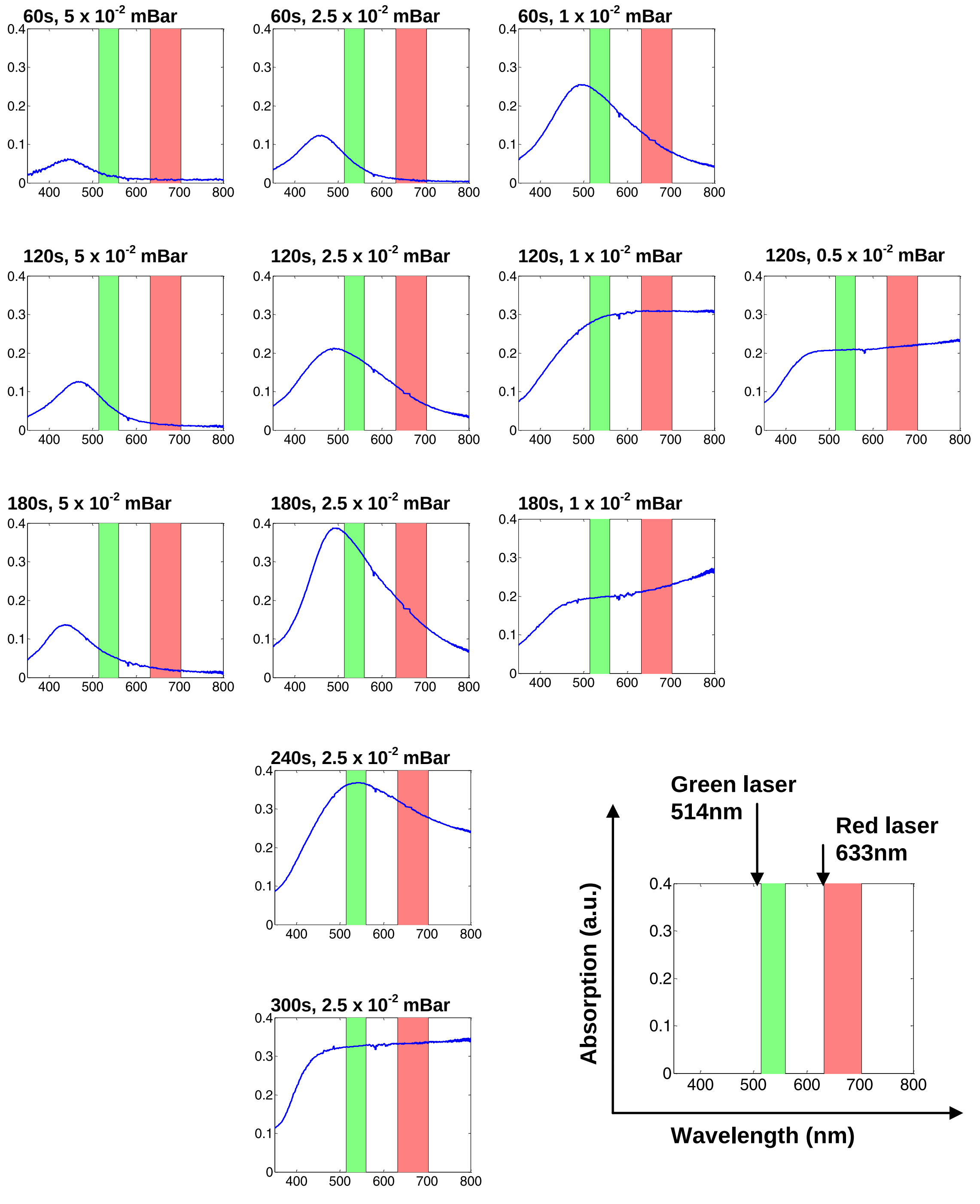

Figure S-2. Light absorption spectrum of the silver particles loaded glass sample. The annotations in each frame indicate the sputtering duration abd working pressure. The green/red marked area in the background are the regions within which the local surface plasma resonates with the excitation lasers (green for 514nm, and red for 633nm) and their corresponding Raman scattered light[12].

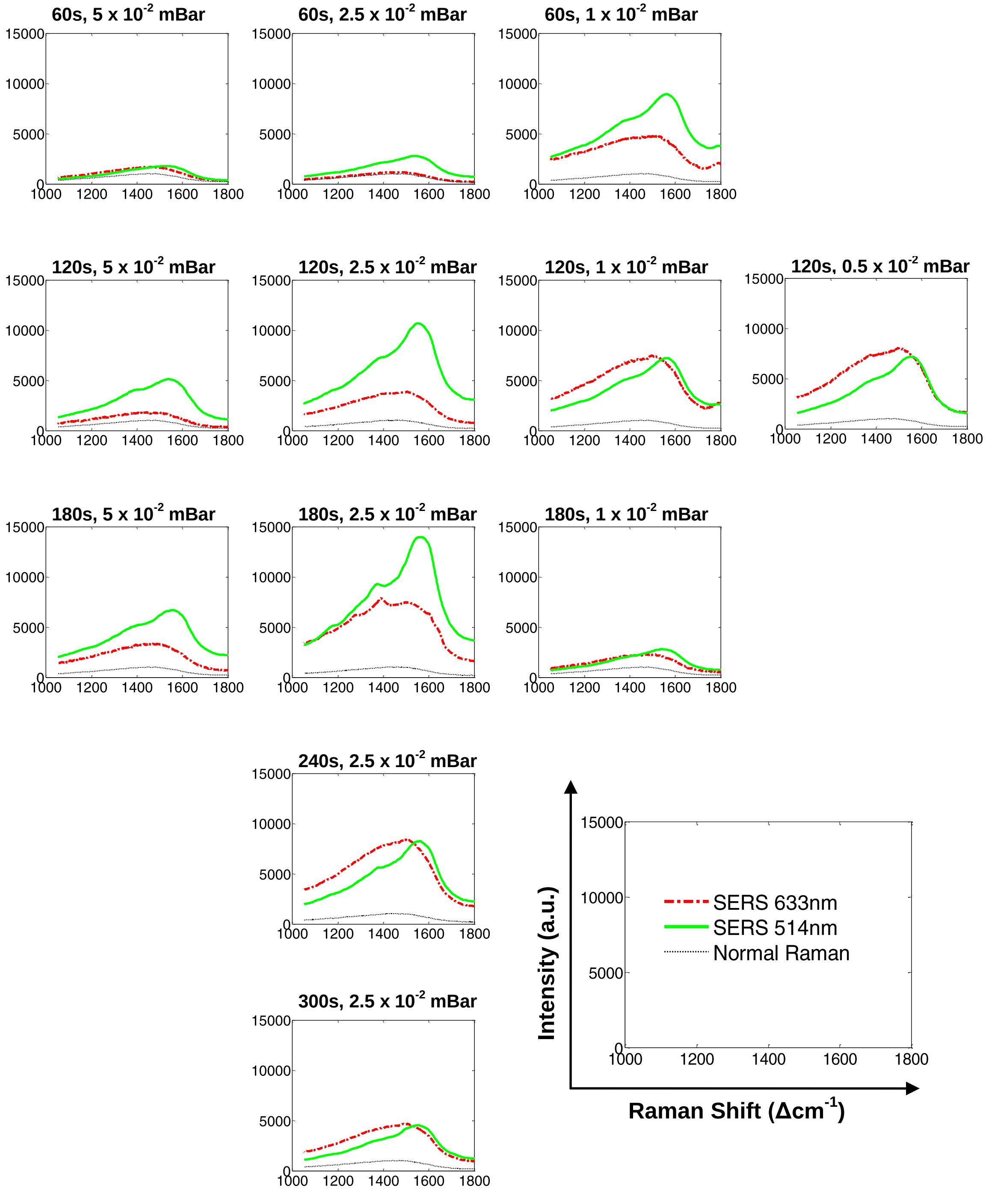

Figure S-3. Enhancement of Raman spectra by loading silver particles with various deposition conditions. The dashed lines are the baselines of carbon before the deposition of silver, red and green indicates the color of incident laser (514nm or 633nm); the green lines are the Raman spectrum with silver loaded. The annotations in each frame are the sputtering duration, working pressure. All baseline peaks are normalized to 1000 counts.

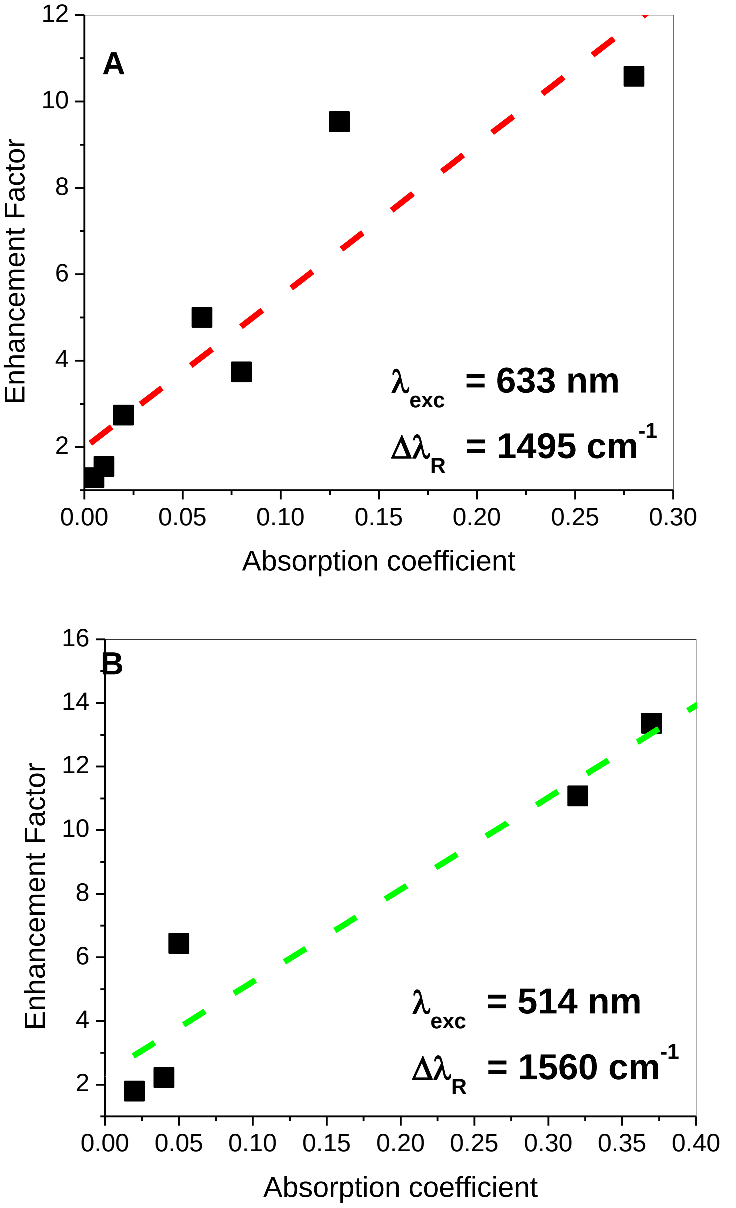

Figure S-4. The correlation between enhancement factors and the light absorption coefficients at the active region of the incident light. (A) Red laser (633nm) was the incident light; the EF was calculated by the peak intensity at 1495cm^{-1}. (B) Green laser (514nm) was the incident light; the EF was calculated by the peak intensity at 1560cm^{-1}. The dashed lines on the plots are presented to guide the eyes.

References

1. E. C. Le Ru, E. Blackie, M. Meyer and P. G. Etchegoin, *Journal of Physical Chemistry C*, 2007, **111**, 13794-13803.
2. R. P. Van Duyne, J. C. Hulteen and D. A. Treichel, *The Journal of Chemical Physics*, 1993, **99**, 2101-2115.
3. W. B. Cai, B. Ren, X. Q. Li, C. X. She, F. M. Liu, X. W. Cai and Z. Q. Tian, *Surface Science*, 1998, **406**, 9-22.
4. C. Ingle, *Spectrochemical Analysis*, Prentice Hall Higher Education, 1999.
5. L. Maya, C. E. Vallet and Y. H. Lee, *Journal of Vacuum Science & Technology a-Vacuum Surfaces and Films*, 1997, **15**, 238-242.
6. A. Merlen, V. Gadenne, J. Romann, V. Chevallier, L. Patrone and J. C. Valmalette, *Nanotechnology*, 2009, **20**, 7.
7. W. Gotschy, K. Vonmetz, A. Leitner and F. R. Aussenegg, *Applied Physics B-Lasers and Optics*, 1996, **63**, 381-384.
8. N. Marechal, E. Quesnel and Y. Pauleau, *Journal of Vacuum Science & Technology a-Vacuum Surfaces and Films*, 1994, **12**, 707-713.
9. R. Gupta, M. J. Dyer and W. A. Weimer, *Journal of Applied Physics*, 2002, **92**, 5264-5271.
10. K. Wasa, M. Kitabatake and H. Adachi, William Andrew Publishing/Noyes.
11. R. Aroca, *Surface enhanced vibrational spectroscopy*, Wiley, 2006.
12. J. Zhao, J. A. Dieringer, X. Zhang, G. C. Schatz and R. P. Van Duyne, *Journal of Physical Chemistry C*, 2008, **112**, 19302-19310.
13. J. A. Dieringer, A. D. McFarland, N. C. Shah, D. A. Stuart, A. V. Whitney, C. R. Yonzon, M. A. Young, X. Y. Zhang and R. P. Van Duyne, *Faraday Discussions*, 2006, **132**, 9-26.